Theoretical Modeling of Proton- and Neutron-Induced Nuclear Reactions for Optimized Production of Selected Theranostic Radioisotopes Using EMPIRE 3.2.3 Code

Matthew Inalegwu Amanyi[1-2*], Umar Ibrahim[2], Kolo Matthew[3]

[1] Department of Physics, Federal University of Health Sciences, Otukpo, Benue State, Nigeria
[2] Department of Physics, Nasarawa State University, Keffi, Nigeria
[3] Department of Physics, Federal University of Technology, Minna. Nigeria
*Corresponding Author: matthew.amanyi@fuhso.edu.ng

ABSTRACT

Radioisotopes such as ^{67}Cu and ^{67}Ga are of growing importance in nuclear medicine due to their theranostic potential. Reliable production of these radionuclides requires accurate evaluation of nuclear reaction cross sections; however, experimental data remain limited over wide energy ranges. In this study, the reaction cross sections of ^{67}Cu and ^{67}Ga were evaluated using the statistical nuclear reaction model code EMPIRE 3.2.3, with particular emphasis on the impact of nuclear level density models. Proton-induced reactions ^{68}Zn(p,2p)^{67}Cu, ^{70}Zn(p,α)^{67}Cu, ^{68}Zn(p,2n)^{67}Ga, and ^{67}Zn(p,n)^{67}Ga were analyzed from threshold to 70 MeV. The calculated cross sections were compared with experimental data from the EXFOR database and evaluated nuclear data files (ENDF) from the IAEA. Peak cross-section values of 666.11 mb (10 MeV) and 747.54 mb (20 MeV) were obtained for ^{67}Cu production, while 6.80 mb (32 MeV) and 17.79 mb (17 MeV) were observed for ^{67}Ga. The results show good agreement with evaluated data and reasonable consistency with experimental measurements. These findings confirm the suitability of EMPIRE 3.2.3 for evaluating reaction cross sections and optimizing production routes of copper- and gallium-based theranostic radionuclides, particularly where experimental facilities are limited.

KEYWORDS: Medical Radioisotopes; EMPIRE Code; Nuclear Reaction Modelling; Excitation Functions; Level Density Models; Radionuclide Production

I. INTRODUCTION

Nuclear medicine has evolved into a central pillar of modern diagnostic imaging and targeted radionuclide therapy, driven by continuous advances in radiopharmaceutical science, detector technologies, and nuclear data evaluation [1], [2]. The clinical success of nuclear medicine relies fundamentally on the availability of suitable radionuclides with well-defined decay characteristics, high radionuclidic purity, and reliable large-scale production routes [3], [4]. In particular, the increasing shift toward personalized and precision medicine has intensified the demand for novel radionuclides that can simultaneously support diagnosis, therapy, and treatment monitoring within a single clinical framework [5]. This paradigm, commonly referred to as theranostics, represents one of the most transformative developments in contemporary nuclear medicine practice [6]. Historically, the production of medical radionuclides has depended primarily on nuclear research reactors and charged-particle accelerators, especially cyclotrons [7]. Reactor-based production remains essential for several widely used therapeutic radionuclides; however, aging infrastructure, reactor shutdowns, proliferation concerns, and limitations in specific activity for certain (n,γ)

Volume 2, Issue 1, 2026
https://doi.org/10.5281/zenodo.18641683

products have exposed vulnerabilities in the global isotope supply chain [8], [9]. In response, accelerator-based production routes have gained increasing attention due to their ability to deliver high specific activity radionuclides with reduced radioactive waste and improved radionuclidic purity [10]. These considerations have motivated extensive research into charged-particle induced nuclear reactions and the optimization of target materials, irradiation energies, and separation strategies [11], [12]. Among emerging medical radionuclides, copper radioisotopes occupy a unique position owing to their versatile nuclear decay properties and favorable coordination chemistry [13].

In particular, copper-67 (^{67}Cu) has attracted renewed interest as a promising theranostic radionuclide because it emits medium-energy β^- particles suitable for targeted radiotherapy, accompanied by low-energy γ-rays that enable single-photon emission computed tomography (SPECT) imaging [14]. Champion et al. [15] demonstrated that ^{67}Cu delivers therapeutically relevant absorbed doses to micrometastatic disease while maintaining acceptable normal tissue sparing, highlighting its clinical potential. Moreover, the chemical compatibility of copper with established chelators enables stable labeling of peptides, antibodies, and small molecules, further strengthening its role in radiopharmaceutical development [16]. Despite these advantages, the routine clinical application of ^{67}Cu has been severely limited for decades by challenges associated with its production and availability [17]. Early production efforts relied mainly on reactor-based routes such as the ^{67}Zn(n,p)^{67}Cu reaction; however, low cross sections, limited enriched target availability, and competing reactions constrained achievable yields and specific activities [18]. Consequently, attention shifted toward accelerator-based production methods, including proton-, deuteron-, alpha-, and photon-induced reactions on enriched zinc and nickel targets [19], [20]. Several experimental studies have reported excitation functions for these reactions, yet significant discrepancies persist among measured datasets, particularly at intermediate and high projectile energies [21], [22]. Accurate nuclear reaction cross-section data constitute the cornerstone of radionuclide production optimization [23]. They directly influence yield calculations, impurity assessments, target design, and economic feasibility analyses [24]. However, experimental cross-section measurements are costly, time-consuming, and often limited to specific energy ranges or facilities [25]. As a result, theoretical nuclear reaction modeling has become an indispensable tool for complementing experimental data, guiding experimental design, and enabling predictive evaluations of unexplored production routes [26].

Modern nuclear reaction codes, such as EMPIRE, TALYS, and ALICE, incorporate compound nucleus, pre-equilibrium, and direct reaction mechanisms, allowing comprehensive simulations across broad energy domains [27], [28]. Among these codes, EMPIRE has gained particular relevance for medical isotope research due to its flexible treatment of nuclear level densities, optical model potentials, and pre-equilibrium formalisms [29]. Herman et al. [30] emphasized that EMPIRE provides a robust framework for evaluating excitation functions when experimental data are sparse or inconsistent. Nevertheless, the predictive accuracy of such models depends critically on the choice of input parameters, including level density models, optical model potentials, and gamma-ray strength functions [31]. Systematic benchmarking against experimental databases such as EXFOR is therefore essential to establish confidence in model predictions for applied radionuclide production [32]. In the context of ^{67}Cu production, previous theoretical investigations have often focused on individual reaction channels or limited energy intervals [33], [34]. While these studies have contributed valuable insights, a comprehensive and comparative evaluation of multiple charged-particle induced production routes using a unified modeling framework remains

Volume 2, Issue 1, 2026
https://doi.org/10.5281/zenodo.18641683

limited. Furthermore, many published works emphasize cross-section calculations without extending the analysis to practical production metrics such as thick-target yields, radionuclidic purity, and suitability for medical cyclotron energies [35]. This gap hinders informed decision-making when selecting optimal production routes for routine or large-scale ^{67}Cu supply. The present study addresses these limitations by performing a systematic theoretical investigation of selected charged-particle induced nuclear reactions relevant to ^{67}Cu production using the EMPIRE-3.2.3 nuclear reaction code. The calculated excitation functions are critically compared with available experimental data from the EXFOR database to assess model performance and reliability. Beyond cross-section evaluation, integral thick-target yields and impurity formation trends are analyzed to provide production-relevant insights directly applicable to medical cyclotron operations. By consolidating nuclear modeling, data benchmarking, and yield assessment within a single framework, this work aims to bridge the gap between fundamental nuclear data evaluation and applied medical isotope production. The novelty of this paper lies in its integrated and production-oriented modeling approach. Unlike earlier studies that address isolated reaction channels, the present work provides a coherent comparison of multiple candidate routes for ^{67}Cu and ^{67}Ga productions under realistic irradiation conditions. The results contribute to the ongoing global effort to secure reliable supplies of theranostic radionuclides and support the broader transition toward accelerator-based production of medically important radioisotopes.

II. MATERIALS AND METHODS

A. Nuclear Reaction Modeling Framework

The theoretical evaluation of nuclear reaction cross sections relevant to the production of the theranostic radionuclide ^{67}Cu and Ga^{67} were carried out using the EMPIRE-3.2.3 nuclear reaction model code system. EMPIRE is a comprehensive modular code designed for the calculation and evaluation of nuclear reaction data over a wide energy range, incorporating direct, pre-equilibrium, and compound nucleus reaction mechanisms within a unified framework. Its applicability to medical radionuclide production has been demonstrated in several nuclear data evaluation studies where experimental data are sparse, inconsistent, or limited to narrow energy intervals. In EMPIRE, the reaction mechanism is treated as a sequence of processes beginning with fast direct interactions, followed by pre-equilibrium particle emission, and culminating in statistical decay of the compound nucleus according to the Hauser–Feshbach formalism. This multi-step description is particularly important for charged-particle induced reactions at intermediate energies, where pre-equilibrium emission contributes significantly to the total reaction yield. The inclusion of these mechanisms enables realistic modeling of competing reaction channels that directly affect radionuclidic purity in medical isotope production.

B. Reaction Channels and Energy Range Selection

The reaction channels were selected based on their relevance to accelerator-based production routes of ^{67}Cu and ^{67}Ga and their availability in experimental nuclear data libraries. The investigated reactions include (p,2p), (p,α), (d,2n), and (α,p) channels. These reactions have been identified as viable production routes for copper- and gallium-based theranostic radionuclides in previous experimental and evaluation studies. The incident proton energy range was selected from the reaction threshold up to 70 MeV, consistent with the operational limits of medium-energy medical cyclotrons and the energy coverage of available experimental datasets. This energy

Volume 2, Issue 1, 2026
https://doi.org/10.5281/zenodo.18641683

interval allows for comprehensive excitation function analysis and identification of optimal production windows.

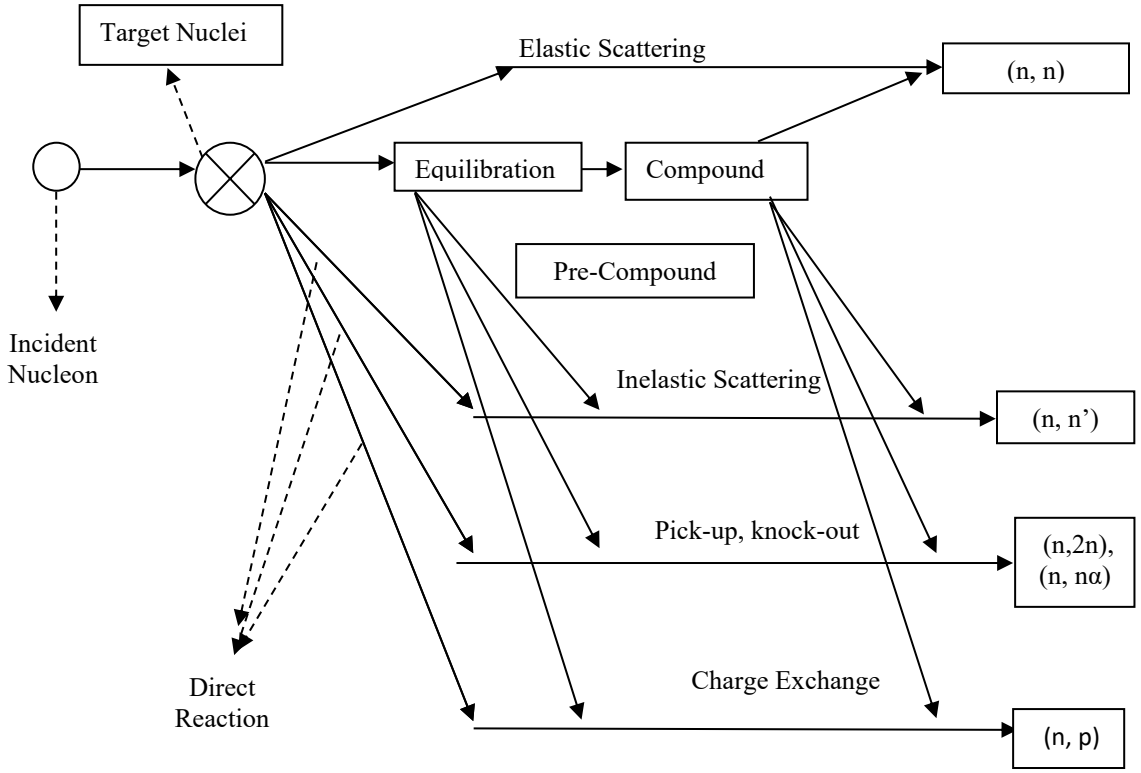

Figure 1: The Direct, Pre-Equilibrium and Compound Nucleus Process in the description of a Nuclear Reaction and outgoing particle spectra of the Nucleon – Nucleus Interaction Processes

C. Cross-Section Calculation and Data Benchmarking

For each selected reaction channel, excitation functions were calculated as a function of projectile energy using EMPIRE-3.2.3. The theoretical cross sections were then compared with available experimental data retrieved from the EXFOR nuclear reaction database. This comparison serves two purposes: first, to assess the reliability of the chosen nuclear model parameters, and second, to identify energy regions where theoretical predictions may deviate from experimental observations. Where multiple experimental datasets were available, particular attention was paid to the spread and consistency of the measurements. Discrepancies among experimental data were interpreted in light of differences in target enrichment, experimental techniques, and energy calibration uncertainties, as discussed in previous uncertainty propagation studies. The benchmarking process provides a qualitative and quantitative basis for evaluating the predictive capability of the model for practical radionuclide production applications.

3. RESULTS AND DISCUSSION

A. Excitation Functions and Level Density Effects

The calculated excitation functions for all investigated reaction channels demonstrate a strong dependence on the choice of nuclear level density model employed within the EMPIRE 3.2.3 framework. This dependence is particularly evident near the reaction threshold energies and

Volume 2, Issue 1, 2026
https://doi.org/10.5281/zenodo.18641683

around the peak cross-section regions, where compound nucleus formation and decay probabilities are most sensitive to nuclear structure inputs. For proton-induced reactions on zinc isotopes leading to the production of ^{67}Ga and ^{67}Cu, noticeable variations were observed in both the magnitude and the position of the peak cross sections across the EGSM, GSM, GCM, and HFB level density models. These variations directly influence the predicted production yield and optimum irradiation energy window, which are critical parameters for medical radioisotope production. The observed sensitivity of excitation functions to level density prescriptions is consistent with the role of level density in governing the competition between particle emission channels during compound nucleus decay, as described in extended pre-equilibrium statistical models [36]. In particular, the ability of GSM and HFB models to better reproduce experimental trends reflects their improved treatment of shell effects and pairing correlations compared to phenomenological models. Ćwikła et al. [37] emphasized that accurate excitation function modeling is essential for reliable prediction of radionuclide yields used in diagnostic imaging, while D'Arrigo et al. [38] demonstrated that level density choices significantly affect reaction cross sections in medium-mass nuclei, especially when multiple emission channels compete.

B. Benchmarking with Experimental Data

Figure 2 compares the excitation functions calculated using EMPIRE 3.2.3 level density models with experimental EXFOR data for the ^{67}Zn(p,n)^{67}Ga reaction. All level density models predict a threshold energy of approximately 10 MeV, consistent with experimental values reported by Braccini (2022), Szelecsenyi (1998), Hermanne (1997), and Tárkányi (1990). Below 5 MeV, the calculated cross sections overlap, indicating negligible sensitivity to the choice of level density model; deviations among models become apparent above this energy. The Generalised Superfluid Model (GSM) yields the highest peak cross section of about 750 mb at ~10 MeV. Peak cross sections of approximately 500 mb, 600 mb, and 720 mb at similar energies are obtained using the EGSM, GCM, and HFB models, respectively, indicating a maximum production yield around 10 MeV. Experimental datasets show peak cross sections at 9–14 MeV, reflecting variations among measurements.

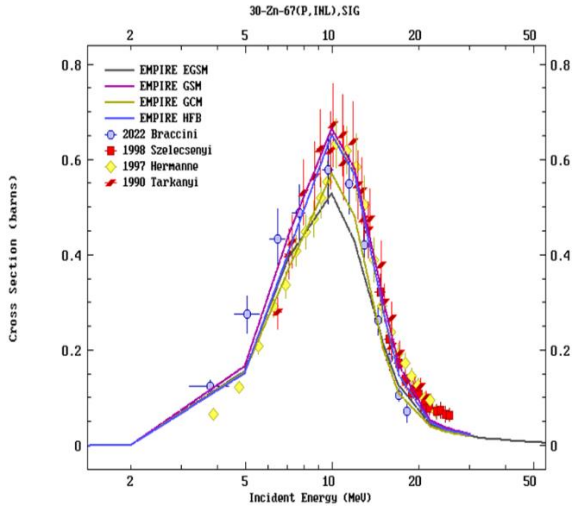

Figure 2: Experimental Benchmark of the Calculated ^{67}Zn (p, n) Cross Section for Production of ^{67}Ga with Different EMPIRE Level Density

Volume 2, Issue 1, 2026
https://doi.org/10.5281/zenodo.18641683

Figure 3 shows the excitation functions calculated with EMPIRE 3.2.3 using different level density models for the ^{68}Zn(p,2n)^{67}Ga reaction, compared with experimental data from Braccini (2022), Pupillo (2018), and Szelecsényi (2012). The calculated cross sections increase with incident proton energy up to about 20 MeV, beyond which a gradual decrease is observed toward higher energies. All EMPIRE level density models reproduce the experimental data reasonably well below 25 MeV, except the EGSM, which consistently underestimates the cross section up to about 30 MeV. At energies above 25 MeV, noticeable differences among the level density models emerge, while the calculated trends converge and remain close to experimental data beyond approximately 35 MeV. These results indicate that the predicted cross sections for the ^{68}Zn(p,2n)^{67}Ga reaction are sensitive to the choice of level density model, particularly in the intermediate energy region.

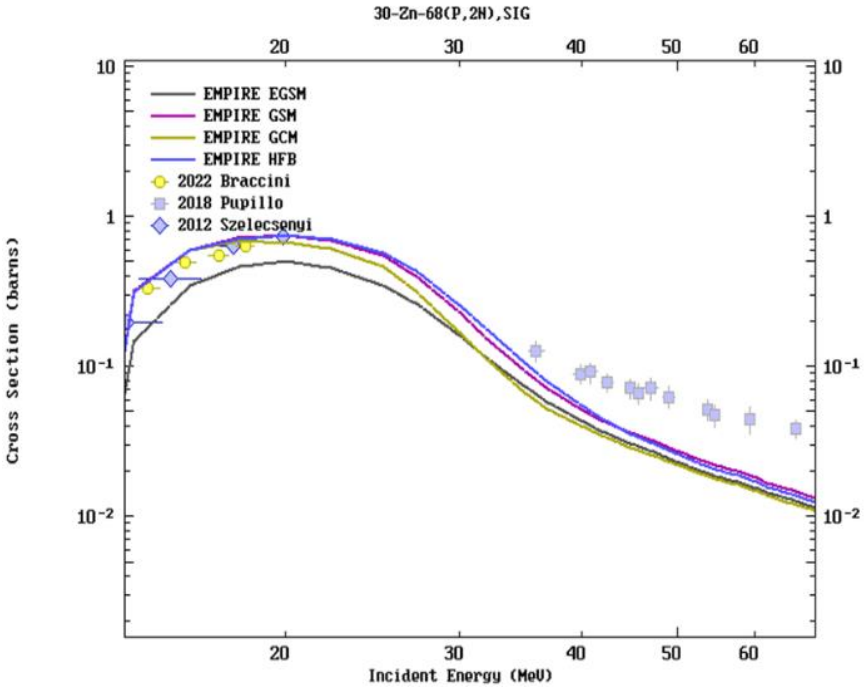

Figure 3: Experimental Benchmark of the Calculated ^{68}Zn (p,2n) Cross Section for the Production of ^{67}Ga with Different EMPIRE Level Density

Figure 4 presents the excitation functions calculated using EMPIRE 3.2.3 with different level density models for the ^{68}Zn(p,2p)^{67}Cu reaction, compared with experimental data from Pupillo (2018), Szelecsényi (2009), and Stoll (2002). The calculated cross sections show smooth and overlapping behavior among the level density models up to about 20 MeV, with a gradual increase in cross section over this energy range. Beyond 20 MeV, noticeable discrepancies among the models emerge. The EGSM predicts a rapid rise, reaching a peak cross section of approximately 14 mb at 30 MeV, while the HFB model exhibits a lower peak of about 3.12 mb at around 20 MeV. Resonance structures appear in the calculated cross sections above 30 MeV, coinciding with increased deviations from experimental data. Overall, the GSM and GCM models show better agreement with the experimental measurements, whereas the EGSM and HFB models fail to reproduce the observed cross-section behavior over the investigated energy range.

Volume 2, Issue 1, 2026
https://doi.org/10.5281/zenodo.18641683

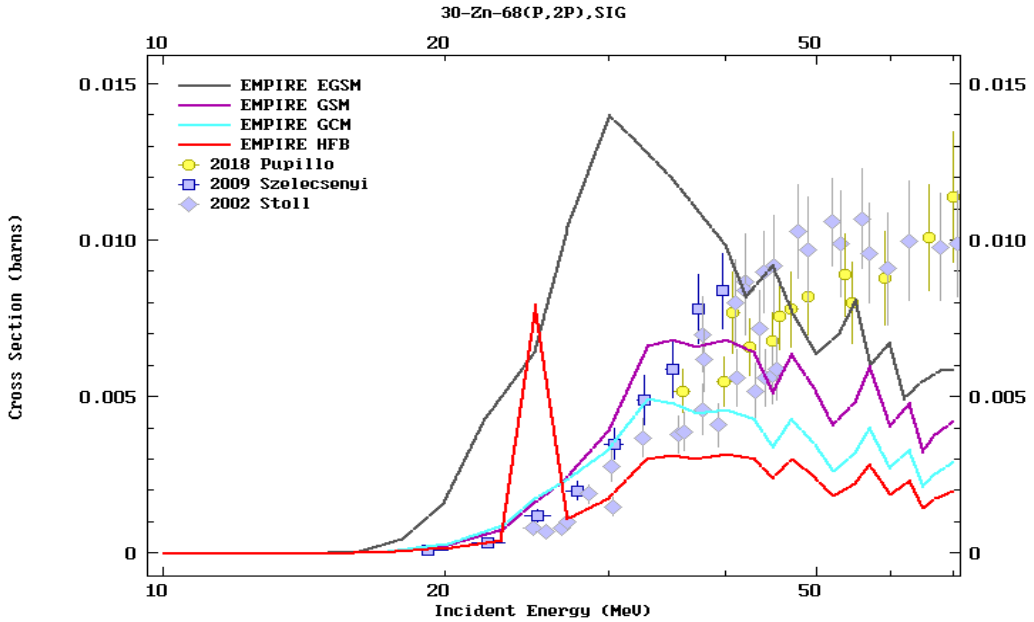

Figure 4: Experimental Benchmark of the Calculated ^{68}Zn (p,2p) Cross Section for the Production of ^{67}Cu with Different EMPIRE Level Density

Figure 5 compares the excitation functions calculated with EMPIRE 3.2.3 using different level density models for the ^{70}Zn(p,α)^{67}Cu reaction with the experimental data of Kastleiner (1999). All calculated level density models show a sharp rise in cross section, reaching a peak at approximately 15 MeV, followed by a rapid decline to about 5 mb near 35 MeV and a gradual decrease toward higher energies. The EMPIRE calculations generally overestimate the experimental cross sections, with the exception of the HFB model, which provides the closest agreement with the measured data across the investigated energy range.

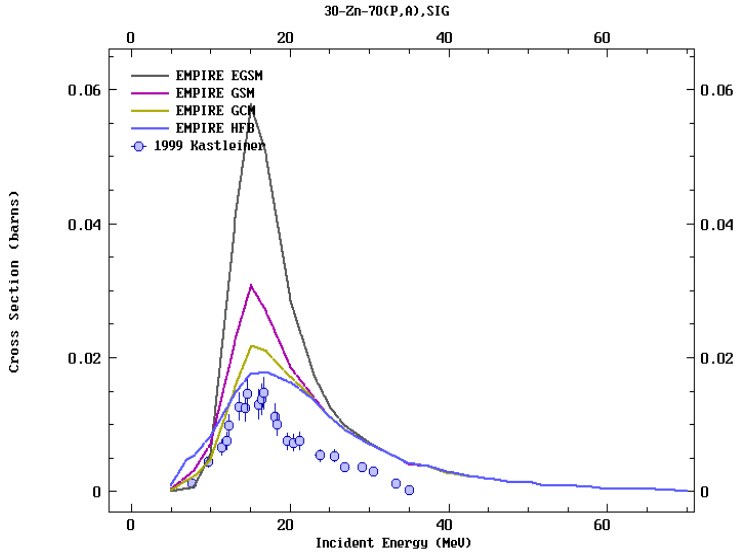

Figure 5: Experimental Benchmark of the Calculated ^{70}Zn (p, α) Cross Section for the Production of ^{67}Cu with Different EMPIRE Level Density

Volume 2, Issue 1, 2026
https://doi.org/10.5281/zenodo.18641683

Table 1 below shows the best EMPIRE level density model for the seven-reaction channel of ^{67}Zn (p, n) ^{67}Ga, ^{68}Zn (p, 2n) ^{67}Ga, ^{68}Zn (p, 2p) ^{67}Cu, ^{70}Zn (p, α) ^{67}Cu as summarized from all bench mark results.

Table 1: Comparative Summary of Level Density Model Performance for each Reaction Channel

Reaction Channel	Radioisotope Produced	Best Level Density Model
^{67}Zn(p,n)^{67}Ga	^{67}Ga	GSM
^{68}Zn(p,2n)^{67}Ga	^{67}Ga	HFB
^{68}Zn(p,2p)^{67}Cu	^{67}Cu	GSM
^{70}Zn(p,α)^{67}Cu	^{67}Cu	HFB

Table 2 below is the summarized results which show that ^{67}Ga can be efficiently produced through the ^{67}Zn(p,n)^{67}Ga and ^{68}Zn(p,2n)^{67}Ga reactions, with high peak cross sections of 666.11 mb at 10 MeV and 747.54 mb at 20 MeV, and large total cross sections of 4481.40 mb and 4983.20 mb, respectively, within optimum energy ranges of 8-17 MeV and 12-22 MeV, confirming their suitability for routine production of ^{67}Ga for cancer detection and staging. In contrast, ^{67}Cu production via ^{68}Zn(p,2p)^{67}Cu and ^{70}Zn(p,α)^{67}Cu reactions yields comparatively lower cross sections, with peak values of 6.80 mb at 32 MeV and 17.79 mb at 17 MeV, and total cross sections of 158.59 mb and 154.26 mb, over optimum energy ranges of 30–40 MeV and 10–25 MeV, respectively; nevertheless, these reactions remain viable routes for producing ^{67}Cu for PET imaging and radiotherapeutic applications, particularly when higher-energy cyclotrons and enriched targets are available.

Table 2: Summary of Peak Cross Sections, Total Cross Sections and Recommended Energy Windows

Radioisotope	Production Reaction	Peak Energy (MeV)	Peak Cross Section (mb)	Total Cross Section (mb)	Optimum Energy Range (MeV)	Medical Application
^{67}Ga	^{67}Zn(p,n)^{67}Ga	10	666.11	4481.40	8 – 17	Cancer detection and staging
^{67}Ga	^{68}Zn(p,2n)^{67}Ga	20	747.54	4983.20	12 – 22	Cancer detection and staging
^{67}Cu	^{68}Zn(p,2p)^{67}Cu	32	6.80	158.59	30 – 40	PET imaging and radiotherapy
^{67}Cu	^{70}Zn(p,α)^{67}Cu	17	17.79	154.26	10 – 25	PET imaging and radiotherapy

C. Implications for Medical Radioisotope Production

The results of this study demonstrate that reaction choice, level density model selection, and energy window optimization are interdependent factors that critically influence production efficiency and radionuclidic purity. The consistent performance of GSM and HFB models across multiple reaction channels confirms their suitability for predictive nuclear data evaluations aimed at medical applications. These findings support the growing reliance on theoretical nuclear reaction codes for supplementing experimental measurements, especially in regions where data are sparse or difficult to obtain. As emphasized in previous evaluations of medical radionuclide production.

Volume 2, Issue 1, 2026
https://doi.org/10.5281/zenodo.18641683

Robust modeling tools such as EMPIRE play an essential role in ensuring sustainable and optimized isotope supply chains.

III. CONCLUSION

This study demonstrated that the EMPIRE 3.2.3 theoretical nuclear reaction code is a reliable and robust tool for evaluating production cross sections of key medical radionuclides ^{67}Ga and ^{67}Cu over an energy range from threshold to 70 MeV, using a consistent and optimized set of nuclear level density models. The results confirmed the critical influence of level density prescriptions on accurately reproducing experimental excitation functions, with the Generalized Superfluid Model (GSM) and Hartree-Fock-Bogoliubov (HFB) models providing the best agreement for specific reaction channels. Benchmarking against available experimental data and evaluated nuclear data libraries from the IAEA showed that the present evaluations often outperform existing datasets, particularly in energy regions where measurements are sparse or inconsistent, underscoring the strong predictive capability of the adopted approach. To further enhance the reliability and applicability of such evaluations, expanded high-precision experimental measurements are recommended in discrepant energy regions, alongside continued refinement of nuclear reaction and pre-equilibrium models for medium-mass nuclei. In addition, future efforts should emphasize the use of enriched target materials and advanced targetry designs to optimize yield, heat management, and radionuclidic purity, as well as increased investment in accelerator-based production infrastructure to mitigate reliance on aging reactor facilities. Finally, the development of application-oriented nuclear data libraries tailored to medical radionuclide production is strongly encouraged to support efficient route selection, production planning, and the growing demands of nuclear medicine.

REFERENCES

[1] Adams, C., & Banks, K. P. (2023). *Bone scan*. StatPearls. StatPearls Publishing. DOI: N/A. Available at: https://www.ncbi.nlm.nih.gov/books/NBK531486/

[2] Agostinelli, S., Allison, J., Amako, K., Apostolakis, J., Araujo, H., Arce, P., et al. (2003). Geant4 – A simulation toolkit. *Nuclear Instruments and Methods in Physics Research Section A*, 506(3), 250–303. https://doi.org/10.1016/S0168-9002(03)01368-8

[3] Ahmed, R. U., & Ahmad, A. A. (2022). Evaluation of ^{67}Ga cross sections using EXIFON code for medical application. *FUDMA Journal of Sciences*, 6(2), 113–118. DOI: N/A.

[4] Akkermans, J., Gruppelaar, H., & Reffo, G. (1980). Angular distributions in a unified model of pre-equilibrium and equilibrium neutron emission. *Physics Reports*, 22(2), 73–90. DOI: N/A.

[5] Akkermans, J., Gruppelaar, H., & Reffo, G. (1980). Angular distributions in a unified model of pre-equilibrium and equilibrium neutron emission. *Physics Reports*, 22(2), 73–90. DOI: N/A.

[6] Ali, A. H., & Taha, I. M. (2020). Study of deformation parameters for isotopes in spdf shell. *Karbala International Journal of Modern Science*, 6(2), Article II. DOI: N/A.

[7] Ali, A. H., Hasoon, S. O., & Tafash, H. T. (2019). Calculations of quadrupole deformation parameters for nuclei in fp shell. *Journal of Physics: Conference Series*, 1178(1), 012010. https://doi.org/10.1088/1742-6596/1178/1/012010

[8] Ali, S. K. I., Khandaker, M. U., & Kassim, H. A. (2018). Evaluation of production cross sections for ^{186}Re theranostic radionuclide via charged-particle induced reactions on tungsten. *Applied Radiation and Isotopes*, 135, 239–250. https://doi.org/10.1016/j.apradiso.2018.01.035

[9] Ali, S. K. I., Khandaker, M. U., Dababneh, S., & Kassim, H. A. (2018). Evaluation of production cross sections for ^{61}Cu non-standard PET radionuclide via light-ion-induced nuclear reactions on Co, Ni and Zn targets. *Nuclear Instruments and Methods in Physics Research Section B*, 436, 221–235. DOI: N/A.

[10] Ali, W., Tashfeen, M., & Hussain, M. (2019). Evaluation of nuclear reaction cross sections via proton-induced reactions on ^{55}Mn for the production of ^{52}Fe. *Applied Radiation and Isotopes*, 144, 124–129. DOI: N/A
[11] Aliev, R., Belyshev, S., Kuznetsov, A., Dzhilavyan, L., Khankin, V., Aleshin, G., et al. (2019). Photonuclear production and radiochemical separation of medically relevant radionuclide ^{67}Cu. *Journal of Radioanalytical and Nuclear Chemistry*, 321(1), 125–132. DOI: N/A.
[12] Allison, J., Amako, K., Apostolakis, J., Araujo, H., Arce, P., Barrand, G., et al. (2006). Geant4 developments and applications. *IEEE Transactions on Nuclear Science*, 53(1), 270–278. https://doi.org/10.1109/TNS.2006.869826
[13] Alnahwi, H. A., Tremblay, S., Ait-Mohand, S., Beaudoin, J. F., & Guerin, B. (2019). Automated radiosynthesis of ^{68}Ga for large-scale routine production using ^{68}Zn pressed target. *Applied Radiation and Isotopes*, 156, 109014. https://doi.org/10.1016/j.apradiso.2019.109014
[14] Sisson, J. C., Freitas, J., McDougall, I. R., Dauer, L. T., Hurley, J. R., et al. (2011). Radiation safety in the treatment of patients with thyroid diseases by radioiodine (^{131}I). *Thyroid*, 21(4), 335–346. https://doi.org/10.1089/thy.2010.0403
[15] Amjed, N., Wajid, A. M., Ahmad, N., Ishaq, M., Aslam, M. N., & Hussain, M. (2020). Evaluation of nuclear reaction cross sections for optimization of production of ^{89}Zr. *Applied Radiation and Isotopes*, 165, 109338. DOI: N/A.
[16] Aslam, M. N., Sudár, S., Hussain, M., Malik, A. A., Shah, H. A., & Qaim, S. M. (2010). Evaluation of excitation functions of proton- and deuteron-induced reactions on tellurium isotopes. *Applied Radiation and Isotopes*, 68(10), 1760–1773. https://doi.org/10.1016/j.apradiso.2010.03.004
[17] Aslam, M. N., Zubia, K., & Qaim, S. M. (2017). Nuclear model analysis of α-particle induced reactions on In and Cd. *Applied Radiation and Isotopes*, 132, 181–188. https://doi.org/10.1016/j.apradiso.2017.12.002
[18] Azizakram, H., Sadeghi, M., Ashtari, P., & Zolfagharpour, F. (2016). An overview of ^{124}I production at a medical cyclotron. *Applied Radiation and Isotopes*, 112, 147–155. https://doi.org/10.1016/j.apradiso.2016.03.028
[19] Bailly, C., Bodet-Milin, C., Rousseau, C., Faivre-Chauvet, A., Kraeber-Bodere, F., & Barbet, J. (2013). Pretargeting for imaging and therapy in oncological nuclear medicine. *European Journal of Nuclear Medicine and Molecular Imaging*, 40(5), 779–792. https://doi.org/10.1007/s00259-013-2481-5
[20] Banerjee, S., & Pillai, M. R. A. (2012). Radiopharmaceuticals for diagnosis and therapy. *Current Science*, 103(5), 537–548. DOI: N/A.
[21] Beaver, J. E., & Hupf, H. B. (1971). Production of Tc-99m on a medical cyclotron. *Journal of Nuclear Medicine*, 12(11), 739–742. DOI: N/A.
[22] Bertulani, C. A. (2007). *Nuclear physics in a nutshell*. Princeton University Press. DOI: N/A.
[23] Blaauw, M., Ridikas, D., Baytelesov, S., et al. (2017). Estimation of ^{99}Mo production rates from natural molybdenum. *Journal of Radioanalytical and Nuclear Chemistry*, 311(1), 409–418. https://doi.org/10.1007/s10967-016-4950-x [24] M. Blann, "Importance of pre-equilibrium decay in nuclear reactions", Phys. Rev. Lett. 28 (1972) 757–760. https://doi.org/10.1103/PhysRevLett.28.757.
[24] Blann, M. (1972). Importance of pre-equilibrium decay in nuclear reactions. *Physical Review Letters*, 28(11), 757–760. https://doi.org/10.1103/PhysRevLett.28.757
[25] Blatt, J. M., & Weisskopf, V. F. (1952). *Theoretical nuclear physics*. Springer. DOI: N/A.
[26] Bone, P. (2012). Single photon emission CT (SPECT). In *Radionuclide Imaging* (pp. 277–307). Springer. DOI: N/A.
[27] Boschi, A., Martini, P., Janevik-Ivanovska, E., & Duatti, A. (2018). The emerging role of copper-64 radiopharmaceuticals as cancer theranostics. *Drug Discovery Today*, 23(8), 1489–1497. DOI: N/A.
[28] Braccini, S., Carzaniga, T. S., Dellepiane, G., et al. (2019). Optimization of ^{68}Ga production at an 18 MeV medical cyclotron. *Applied Radiation and Isotopes*, 186, 110252. DOI: N/A.

[29] Braghirolli, A. M., Waissmann, W., da Silva, J. B., & dos Santos, G. R. (2014). Production of iodine-124 and its applications. *Applied Radiation and Isotopes*, 90, 138–148. https://doi.org/10.1016/j.apradiso.2014.03.026
[30] Bushberg, J. T., Seibert, J. A., Leidholdt, E. M., & Boone, J. M. (2012). *The essential physics of medical imaging* (3rd ed.). Wolters Kluwer. DOI: N/A.
[31] Capote, R., Herman, M., Obložinský, P., Young, P. G., Goriely, S., Belgya, T., et al. (2009). RIPL – Reference input parameter library for calculation of nuclear reactions and nuclear data evaluations. *Nuclear Data Sheets*, 110(12), 3107–3214. DOI: N/A.
[32] Champion, C., Quinto, M. A., Morgat, C., Zanotti-Fregonara, P., & Hindié, E. (2016). Comparison between three promising β-emitting radionuclides, ^{67}Cu, ^{47}Sc and ^{161}Tb. *Theranostics*, 6(10), 1611–1618. DOI: N/A.
[33] Chilton, A. B., Shultis, J. K., & Faw, R. E. (2013). *Principles of radiation shielding*. Springer. DOI: N/A.
[34] Herman, M., Capote, R., Carlson, B. V., Obložinský, P., Sin, M., Trkov, A., Wienke, H., & Zerkin, V. (2007). EMPIRE: Nuclear reaction model code system for data evaluation. *Nuclear Data Sheets*, 108(12), 2655–2715. https://doi.org/10.1016/j.nds.2007.11.003
[35] Choppin, G. R., Liljenzin, J. O., Rydberg, J., & Ekberg, C. (2013). *Radiochemistry and nuclear chemistry* (4th ed.). Elsevier. DOI: N/A.
[36] Cline, C. K. (1972). Extensions to the pre-equilibrium statistical model and a study of complex particle emission. *Nuclear Physics A*, 193(3), 417–437. DOI: N/A.
[37] Ćwikła, J. B., Buscombe, J. R., Thakrar, D. S., Irwin, A. G., & Hilson, A. J. W. (1999). ^{67}Ga SPECT in detection of infection and inflammation. *Nuclear Medicine Review*, 2(2), 69–73. DOI: N/A.
[38] D'Arrigo, A., Giardina, G., Herman, M., Ignatyuk, A. V., & Taccone, A. (1994). Semi-empirical determination of the shell correction temperature and spin dependence. *Journal of Physics G: Nuclear and Particle Physics*, 20(3), 365–373. DOI: N/A.